IUST
Iran University of Science and Technology

Iranian Journal of Electrical and Electronic Engineering

Journal Homepage: ijeee.iust.ac.ir

Research Paper

Grid Interconnection of Solar and Battery System Using an Asymmetrical T-Type Multilevel Inverter to improve Conversion Efficiency with Reduced THD

S. K. Gudey*(C.A.) and S. Andavarapu*

Abstract: A three-phase dual-port T-type asymmetrical multilevel inverter (ASMLI) using two sources, solar forming the high voltage level and the battery forming the low voltage level, is considered for grid interconnection. A vertical shifted SPWM is used for the ASMLI circuit. A transformerless system for grid interconnection is achieved for a 100-kW power range. A well-designed boost converter and a Buck/Boost converter is used on the front side of the inverter. Design of battery charge controller and its controlling logic are done and its SOC is found to be efficient during charging and discharging conditions. A closed-loop control using PQ theory is implemented for obtaining power balance at 0.7 modulation index. The THD of the current harmonics in the system is observed to be 0.01% and voltage harmonics is 0.029% which are well within the permissible limits of IEEE-519 standard. The power balance is found to be good between the inverter, load, and the grid during load disconnection for a period of 0.15s. A comparison of THD's, voltage, current stresses on the switches, and conduction losses is also presented for a single-phase system with respect to a two-level inverter which shows improved efficiency and low THD. Hence this system can be proposed for use in grid interconnection with renewable energy sources.

Keywords: Asymmetrical Multilevel, Battery, Efficiency, Solar, THD.

1 Introduction

THE requirements of high efficiency and good power quality involve research of new converter or inverter topologies with lowest cost. The photovoltaic inverters [1-3] work at low efficiency when operating at higher switching frequencies which is desirable to reduce the component size and cost. But with increased switching frequency, losses are increased and also the cooling/heat sink requirement becomes necessary. The switches experience voltage and current stress and cause high Electromagnetic Interference (EMI) effect. In view of these all aspects, present research is focused towards the development of new topologies of multilevel inverters for grid interconnection of renewable energy. Multilevel inverters (MLI) are increasingly being used due to distributed generation. The key role of multilevel converters in applications like adjustable speed drives, reactive power compensation, HVDC transmission, electric vehicles, induction heating, back-to-back intertie, UPS for computers, and grid interconnection [1].

In this work, the input solar energy operating with maximum power point technique (MPPT) algorithm [4-6] combines with boost converter [7, 8] to step up the low voltage and also to maintain a constant DC link voltage. Parallel to this, a battery [7] source with a charge controller is used to store the energy. AT-type Asymmetrical multilevel converter (AS-MLI) topology presented in [9-12] is chosen for the system analysis. The T-type inverter being a transformerless system is cost-effective [13]. The controller used for this converter is a vertically shifted sinusoidal pulse width modulation (SPWM) technique [12]. The output of the

Iranian Journal of Electrical and Electronic Engineering, 2021.
Paper first received 14 April 2020, revised 26 December 2020, and accepted 15 January 2021.
* The authors are with the Department of Electrical and Electronics Engineering, Gayatri Vidya Parishad College of Engineering (Autonomous), Visakhapatnam, Andhra Pradesh, India.
E-mails: satishgudey13@gmail.com and sreedhar.andavarapu14@gmail.com.
Corresponding Author: S. K. Gudey.
https://doi.org/10.22068/IJEEE.17.3.1857

converter is fed to an *LCL* filter in order to remove the harmonic content from it during grid interconnection. The grid is interconnected [14-16] to the system to supply power to the grid and also to the loads at the distribution side of the system. The load is operated for certain time interval and disconnected in order to check the system stability. The battery with charge controller acts as a backup energy source to the existing system mostly used at the distribution generation systems. By using T-type ASMLI at the distribution level, total harmonic distortion (THD) can be reduced. An improvement in the conversion efficiency with reduced filter size can be achieved. The system performs a transformerless operation for grid interconnection for 100 kW range. The contributions presented in this work include

- ❖ A three-phase dual-port T-type Asymmetrical multilevel inverter (DP-ASMLI) using two sources, high voltage level from solar and the battery forming the low voltage level is considered for grid interconnection.
- ❖ The system performs transformerless operation for grid interconnection for 100 kW range.
- ❖ A vertical shifted SPWM is used for ASMLI circuit. A closed-loop control using *PQ* theory is implemented for obtaining power balance at 0.7 modulation index.
- ❖ Design of front end converter, inverter, and the filter parameters.
- ❖ Battery operation (charging and discharging) in safe conditions (10%-90%) with the help of - SOC code.
- ❖ At the source side, controlling the battery with and without solar power as input.
- ❖ On the load side, the switching of T- type ASMLI converter with vertical shifted SPWM during on & off load conditions is performed. Using PQ- theory, efficient power-sharing is obtained between inverter to load and grid.
- ❖ A comparison of THD's, voltage, current stresses on the switches and conduction losses are presented for a single-phase system with a two-level inverter which shows improved efficiency and low THD for use in grid interconnection with renewable energy sources.

Section 2 addresses the design and operation of a three-phase T-type ASMLI. Subsections 2.1, 2.2, and 2.3 cover the design of boost converter parameters, buck/boost charge controller parameters, *LCL* filter design. The working T-type ASMLI is presented in Section 3. The closed-loop operation using generalized theory of instantaneous reactive power in three-phase circuits also known as *pq*-theory for AS-MLI is presented in Section 4. The results and discussions with two different cases of inverter operation are discussed in Section 5. Section 6 presents the comparison of a single-phase AS-MLI with a two-level inverter. Conclusions and future scope are presented in Section 7.

2 Design and Operation of a Three-Phase T-Type MLI

The overall system block diagram is shown in Fig. 1(a). Fig. 1(a) shows the input DC source i.e. solar

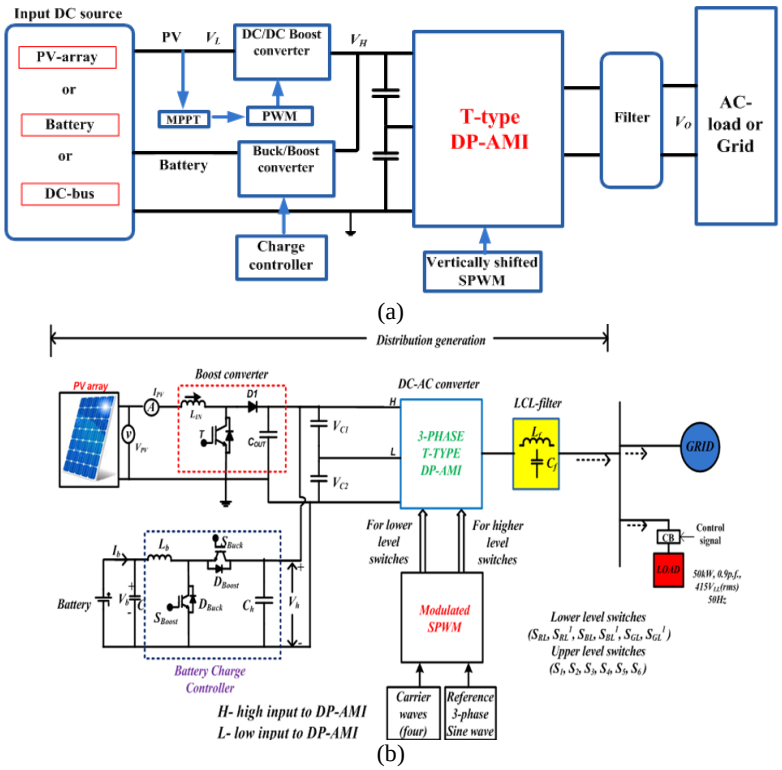

Fig. 1 a) Schematic diagram and b) Proposed system.

Table 1 Specifications of the proposed system.

Parameter	Value
V_{rms}(*L-L*)	415 V
Frequency	50 Hz
Battery capacity	300 V, 2.0 kWh
PV open circuit voltage	300 V (approx.)
IGBT and DIODE ratings	1200 V, R_{on} = 0.01Ω, R_{off} = 1 MΩ
Switching frequency f_{sw}	5 kHz
Load	50 kW with 0.9 power factor lag

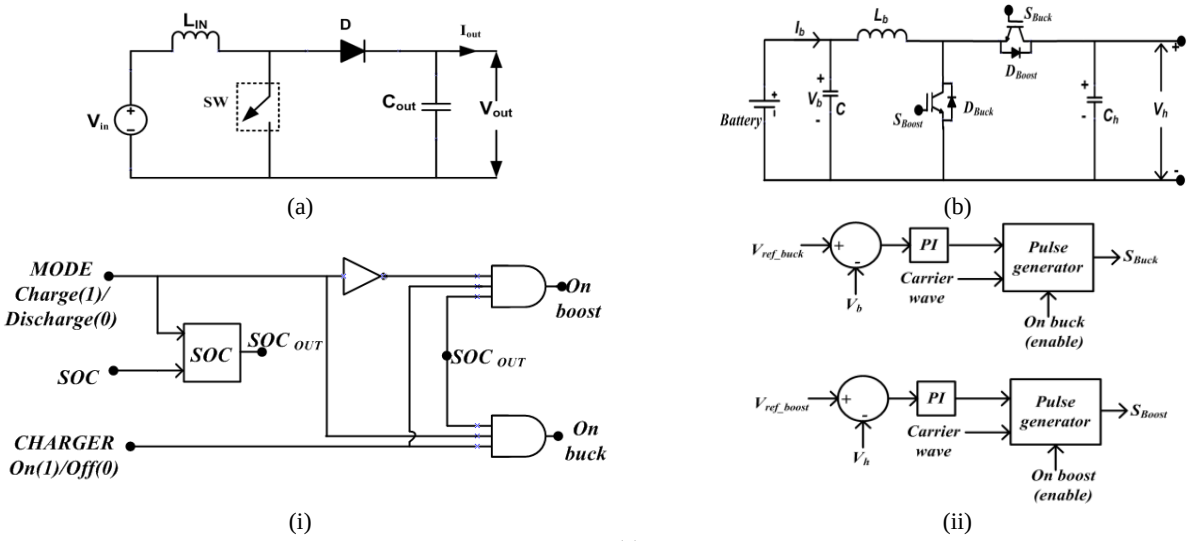

Fig. 2 a) Circuit diagram of the boost converter, b). Battery with the buck/boost charger, and c) (i) Upper level & (ii) lower level control of battery charger.

energy operating with MPPT algorithm combines with boost converter to step the low voltage and also to maintain the link voltage constant for various input levels of inverter. A high voltage source i.e. a battery in parallel with the bidirectional converter is also used to store the energy if the generation is surplus/more than the demand. It also supplies power when the solar input fails to meet the load demand. The system consists of boost converter and Buck/Boost charge controller at front end of inverter. The *LCL* filter is present on the output side of the three-phase dual-port Asymmetrical Multilevel inverter (DP-ASMLI) [12]. A 50kW load and grid operating at 415$V_{L\text{-}L}$ (RMS), 50Hz connected after the filter. Vertical shifted SPWM with *pq*-theory is used for controlling the switches of the inverter. The system operation with solar as input and battery in charging condition during the day time is presented. The system performance is observed on the grid side. In the absence of solar system with battery in the discharging condition is also observed. During both conditions, the system performance is observed by switching to an inductive load (rated as 50kW with 0.9 pf lag) for a small duration of 0.15s. The system specifications are shown in Table 1. The proposed system with controller is shown in Fig. 1(b).

2.1 Design of Boost Converter Parameters

The generated photovoltaic (PV) power with low voltage levels are stepped up with the help of boost converter as shown in Fig. 2(a) [4, 5]. The parameters (L_{IN} &C_{OUT}) of the boost converter are properly designed to obtain low ripple in the output voltage and inductor current. Continuous mode of operation is assumed.

The design of the boost converter is performed based on the following calculation. The output voltage equation is given as follows: (SW = MOSFET or IGBT, *D*(duty ratio) = 0.5 & V_{IN} = 300V)

$$V_{Out} = \frac{V_{IN}}{1-D} = \frac{300}{1-0.5} = 600 \tag{1}$$

For good estimation, ΔI_L must be 20% to 40% of I_{out} (A)

$$\Delta I_L = (20-40)\% I_L;\ L_{IN} = \frac{V_{IN} \times D}{\Delta I_L \times f_S} H \tag{2}$$

$$\Delta V_O = ESR\left(\frac{I_O}{1-D} + \frac{\Delta I_L}{2}\right) V;\ C_{OUT} = \left(\frac{I_0 \times D}{f_S \times \Delta V_O}\right) F \tag{3}$$

Using (1) to (3), one can obtain the L_{in} and C_{out} components of the boost converter. To maintain output voltage with less ripple, the value of the capacitor should be very high. L_{in} and C_{out} are obtained as 0.166mH and 25mF at a switching frequency of 15kHz.

2.2 Design of Buck/Boost Charge Controller parameters

Battery is used as the backup in the system for energy storage [7]. The charge controller, also known as a buck/boost controller, shown in Figure 2(b) is used with the battery to operate it in a normal condition. It depends on state of charge of the system. The values of the converter parameters (*L*&*C*'s) are calculated using the formulas (4)-(6) [13]

$$L_b = \frac{D(1-D)^2 R}{2f_S} \tag{4}$$

$$C = \frac{1-D}{8L \times \left(\Delta V_o / V_o\right) \times f_S^2} \tag{5}$$

$$C_h = \frac{V_o \times D}{\Delta V_o \times R \times f_S} \tag{6}$$

The switches indicated as buck or boost at their suffixes, perform the respected operation. The first stage is known as upper-level control and second one as lower level control which are shown in Fig. 2(c); (i) and (ii). The operation of the charge controller depends on the mode of operation and charger mode of operation. These are the input commands to the SOC of the charge controller; the SOC develops signals based on the program implemented to operate the battery SOC between 5% to 100% and the pulses are given to the switches of the buck/boost converter. The values of the charge controller are obtained as L_b = 0.25mH, C = 6mF, C_H = 5mF, respectively operating at 5 kHz.

2.3 Design of LCL Filter parameters

The filter which is preferred for grid interconnection is an *LCL* type [13] which is shown in Fig. 3. It reduces the amount of current ripple that should be injected to the grid. The value of damping is chosen depends on the existence of the oscillations within the system.

$$Z_b = \frac{V_{LL}^2}{P_n} \text{ and } C_b = \frac{1}{\omega_g Z_b} \tag{7}$$

$$L_1 = \frac{V_{DC}}{6 f_{SW} \Delta I_{L\max}} \tag{8}$$

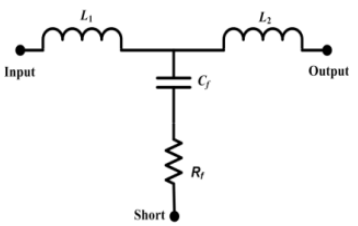

L_1 = inverter side inductor,
L_2 = grid side inductor
C_f = filter capacitor (5% of C_b)
R_f = filter resistance,
K_a = 0.2(20%), attenuation factor,
ω_{res} -resonance frequency
P_n- rating of the overall system.
V_{LL}- line to line RMS voltage.

Fig. 3 LCL filter for grid interconnection.

$$L_2 = \frac{\sqrt{\frac{1}{K_a^2}+1}}{C_f F_{SW}^2} \tag{9}$$

$$\omega_{res} = \sqrt{\frac{L_1+L_2}{L_1 L_2 C_f}} \text{ and } R_f = \frac{1}{3\omega_{res} C_f} \tag{10}$$

The values of the L_1 and L_2 are calculated using the values of base impedance obtained using the system rating [16].The values of L_1 = 1.59mH, L_2 = 1.26mH, C_f = 9.4mF, and R_f = 0.099Ω. L_1 is slightly higher than L_2.

3 Operation of a Dual-Port T-Type MLI Converter

The block diagram of a dual-port T-type MLI converter is shown in Fig. 4. The operation of the converter is explained by taking one phase of the three-phase system. The converter consists of four switches in each leg/phase, two switches for low-level voltage generation represented by S_{RL} and S_{RL}^1. The high-level switches are represented as like conventional converter [9-12]. The low-level switches are connected to the midpoint of the capacitor. The operation of T-type inverters is explained by taking the single-phase with four switches marked in red color. The vertical shifted SPWM technique is used to generate pulses to the switches of the converter which is shown in Fig. 5.

Vertical shift SPWM [11, 12] works is a high-frequency switching mechanism used in power converter switching. It generates pulses when the reference sine waveform signal amplitude is higher than the carrier signal. The vertically shifted SPWM has categories like (i) All carriers are in phase (Ph-disposition) All carriers above the zero reference are in phase, but in opposite with those below (PO-disposition), (iii) All carriers are alternatively in opposition (APO-disposition). The switching is generated using the vertically shifted SPWM which is of opposite phase disposition type. Fig. 5 is represented for understanding the vertical SPWM. It shows the operation of the vertical SPWM. The switching pulses are also presented. During the starting of the sine wave from origin the pulses are generated to low level

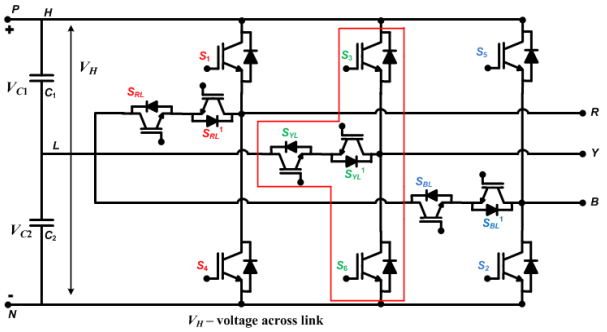

Fig. 4 T-type converter block diagram.

(a)

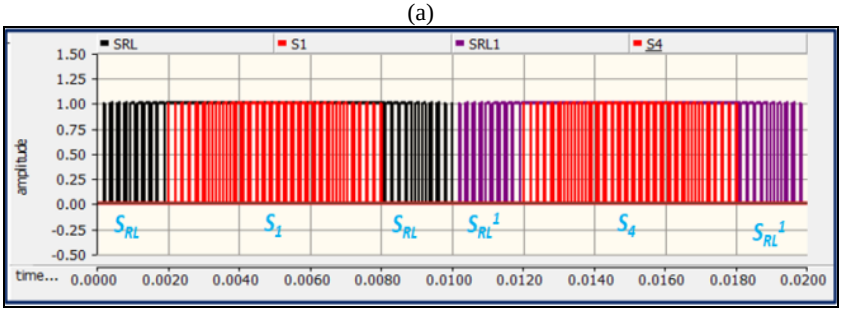

(b)

Fig. 5 a) Vertical shifted SPWM and b) Switching pulses to one leg of the three-phase switches.

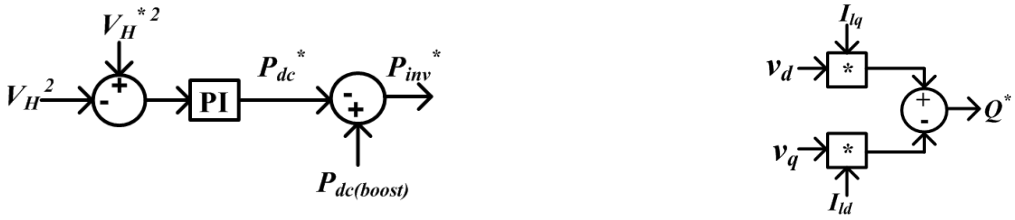

(a) (b)

Fig. 6 a) Active power regulation and b) Reactive power regulation.

switch(S_{RL}^1), after reaching half magnitude of the sine wave the higher level switches in the converter turn's on [17-20].

During the positive half, the switch S_{RL} is turned on and after certain interval S_1 is turned on, the higher-level of voltage is observed in this interval. S_{RL} comes into conduction when the switch S_1 is turned off. Similarly, the switches S_{RL}^1 and S_4 are operated during the negative half cycle.

The modulation index M_a is given by (11) where V_r is reference wave magnitude, and V_c is 4 times that of one carrier wave magnitude and M_a varies as 0.7, 0.8, 0.9, and 1.0 by varying the carrier wave amplitude. A trade-off in selecting the switching frequency based on the size of filter components, ratings of switches and cost economics is to be considered.

$$M_a = \frac{V_r}{V_c} \tag{11}$$

4 Closed Loop Analysis Using PQ-Theory

The three-phase (a, b, and c) quantities are converted into synchronous quantities (d, q) and the transforming equation is given in (6).

$$\begin{pmatrix} F_d \\ F_q \end{pmatrix} = \sqrt{\frac{2}{3}} \begin{bmatrix} \cos\theta & \cos\left(\theta - \frac{2\Pi}{3}\right) & \cos\left(\theta + \frac{2\Pi}{3}\right) \\ -\sin\theta & -\sin\left(\theta - \frac{2\Pi}{3}\right) & -\sin\left(\theta + \frac{2\Pi}{3}\right) \end{bmatrix} \begin{bmatrix} F_a \\ F_b \\ F_c \end{bmatrix} \tag{12}$$

The reference signals for the analysis of *pq*-theory are taken from the grid and load as shown in Fig. 1(b). The grid voltages are taken as voltage references and the current signals are taken from both load and from the grid. The load currents are taken for reactive power regulation. The active power generated by the inverter is found by the amount of current that is injected into the grid or load [21-23]. This is given by I_d (d-axis) component value of the inverter. The current component indirectly depends on the DC link voltage because it represents the rate of change of energy stored in that link which is to be transferred. Figs. 6(a) and (b) shows the active and reactive power reference generation.

The *PQ*- theory analysis is applied to obtain

references of active P_{inv}^* and reactive powers Q^*. The analysis is performed on the DC components of the system.

$$\begin{bmatrix} i_d^* \\ i_q^* \end{bmatrix} = \frac{1}{v_d^2 + v_q^2} \begin{bmatrix} v_d & v_q \\ -v_q & v_d \end{bmatrix} \begin{bmatrix} P_{inv}^* \\ Q^* \end{bmatrix} \tag{13}$$

$$v_d^1 = PI\left(i_d^* - i_d\right) \tag{14}$$

$$v_q^1 = PI\left(i_q^* - i_q\right) \tag{15}$$

$$v_d^* = v_d + v_d^1 - L_f \omega i_q \tag{16}$$

$$v_q^* = v_q + v_q^1 + L_f \omega i_d \tag{17}$$

From (7)-(11), the voltage reference in *dq* format is generated and again transformed into three-phase components. The *dq* current references (I_d* & I_q*) are generated with the available active and reactive power reference components (P_{inv}* & Q*). These are compared with their actual values and the error is given to a PI controller. The reference voltage components in *dq*-format are obtained as V_d* and V_q*. From this analysis, the voltage reference in *dq* format is generated. These are again transformed into the three components using inverter clark and park expressions. The three-phase references are given to the vertically shifted SPWM. The pulses to the respective switches are generated by comparing the reference with the four carrier waves.

5 Simulation Results and Discussions

The rating of the solar panel with the open-circuit voltage of 0.84V/cell and short circuit current of 2.5A/cell are taken. For 90kW with an input voltage of 300V system, a 36 cell configuration with 10 modules in series and 120 module strings in parallel is considered. The panel is operated at STC which are irradiance of 1000 W/m^2 and temperature of 25°C. The input voltage is shown in Fig. 8 (a). The switch of the boost converter is controlled by the MPPT controller which is operated with Perturb and Observe (P&O) algorithm. The output voltage is maintained at 600V for high level and 300V for low-level inputs for the T-type inverter by using capacitors. The case studies are presented for validating the work as (a) during load disconnection of 0.15 s, the power balance is observed with both battery and PV as the source of power supply, (b) load disconnected with only battery as a source i.e. during night times or during emergency conditions.

5.1 Case1: Load Disconnection for 0.15s

The load is rated with 50kW and the remaining generated power is supplied to the grid. The PV system is designed to supply 50kW (approx.) to load and remaining to the grid (40kW). PV system with T-type converter is rated above 90kW.

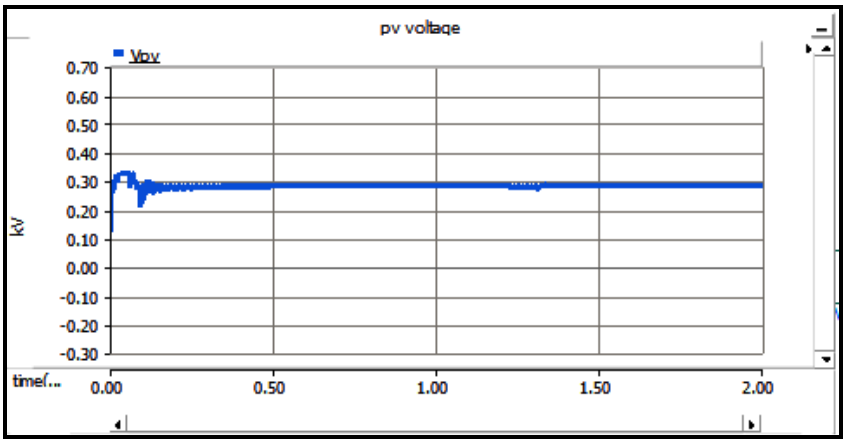

(a)

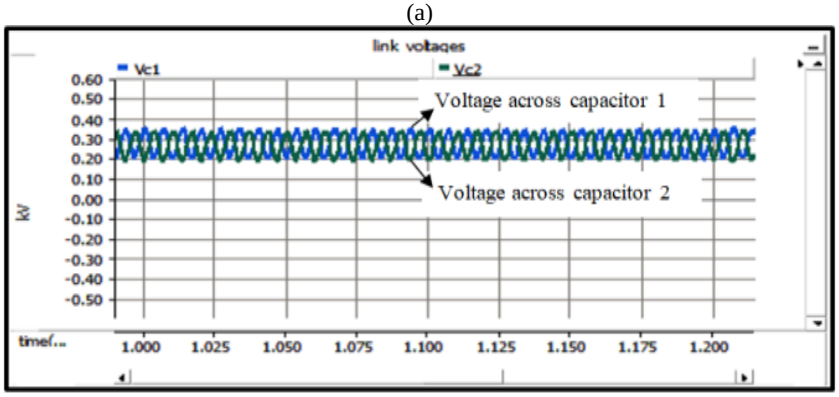

(b)

Fig. 7 a) Input voltage of the PV panel and b) Voltages across the link capacitors C_1 and C_2.

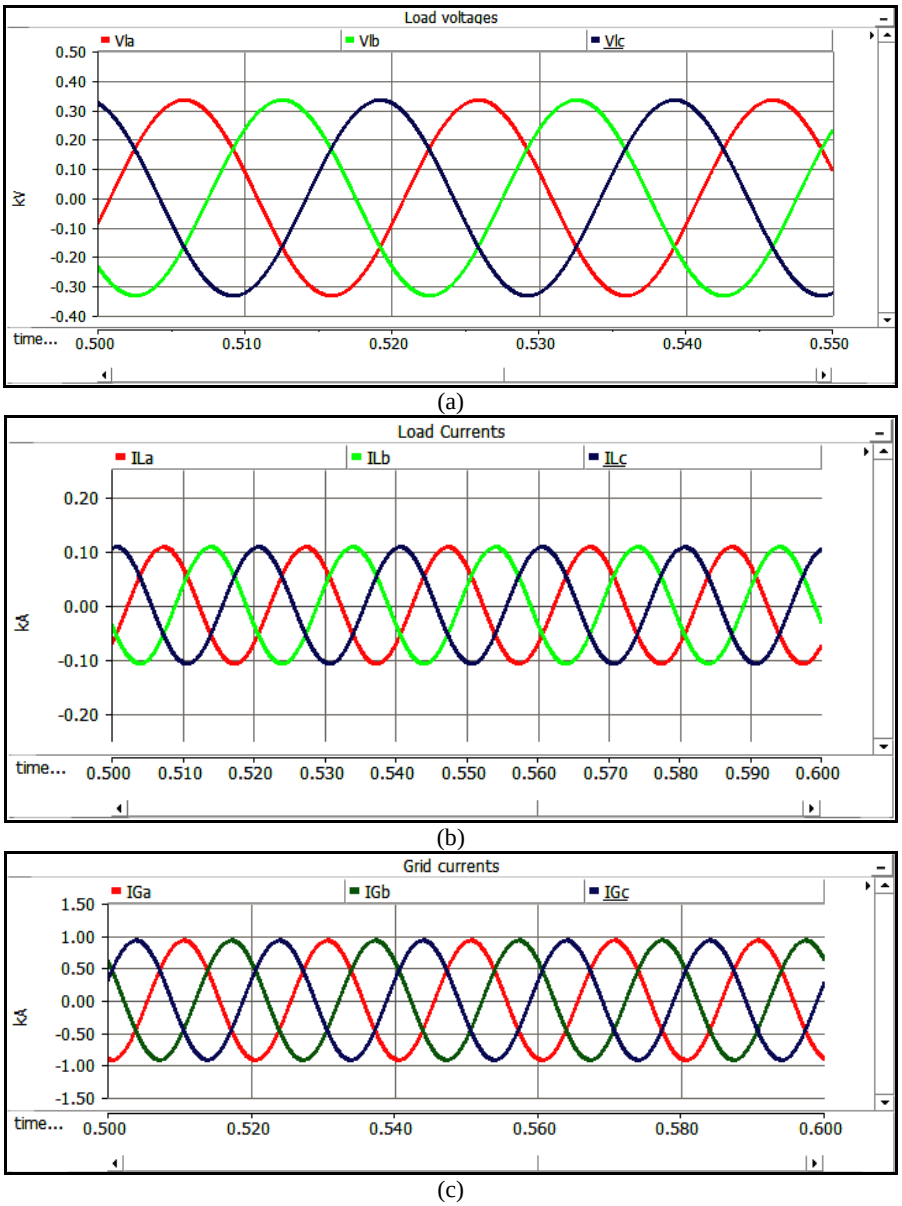

Fig. 8 a) Three-phase load voltages, b) Three-phase load currents, and c) Three-phase grid currents.

Fig. 7(a) shows the input PV panel voltage which is of 300V with minimum ripple. For this, 10 series modules (30V each) configuration is taken. The link voltages are indicated in Fig. 7(b) with a ripple of 3%, this can be reduced by increasing the capacitor value. Each link voltage is of 300V (average) approximately. The two link voltages are used as two input voltages to the T-type inverter. From Fig. 8 (a), it is observed that the load voltage waveforms of 415V (RMS) are pure sine waves with less THD. The three-phase load currents are shown in Fig. 8(b). The grid current of a three-phase system is observed in Fig. 8(c). The line-to-line RMS voltage of the three-phase system is 415V. The breaker is used to isolate the load for the particular time period and reconnect it again. To check the system stability performance, this operation is done.

The waveforms of three-phase load when load is disconnected are observed in Fig. 9(a) and (b). These indicate no power flow from source to the load during the shutdown (t=0.6s to 0.75s) of the load. The current waveform is taken after breaker. The three-phase load current is shown in Fig. 9(a) and the voltage and current of one of the three-phase of the system are shown in Fig. 9(b). The load is connected again after a time period of 750ms. From Fig.10 (a), it is clear that the power flow is balanced in between load, grid, and converter. During the period of 0.6 to 0.75sec the load is disconnected, and then the power (50kW) is supplied to the grid. After 0.8sec again the load comes into operation. Then the power balance is maintained i.e. 90kW. The load absorbs 24kVAr power and the rest is given to the grid. The reactive power requirement depends on the load. The instant at which the load is disconnected and the power supplied by the inverter is taken by the load are shown clearly in Fig. 10(b).

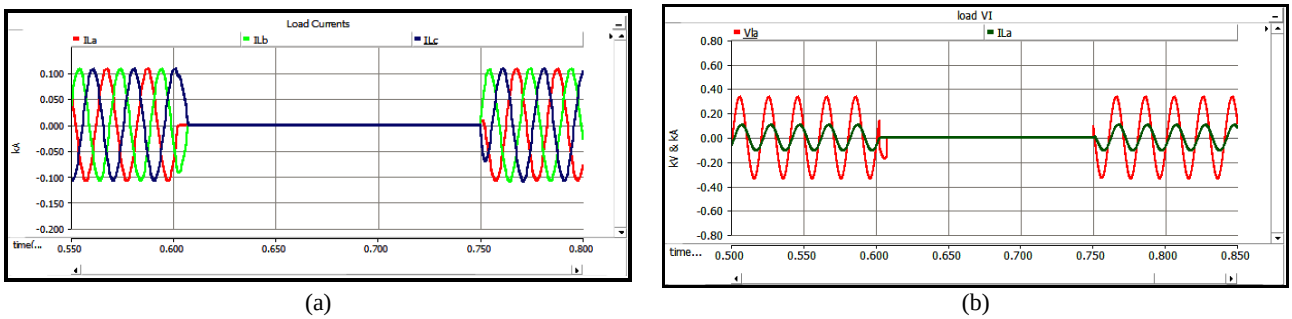

(a) (b)

Fig. 9 a) Three-phase load currents when load is disconnected and b) Single-phase load voltage and current when load is disconnected.

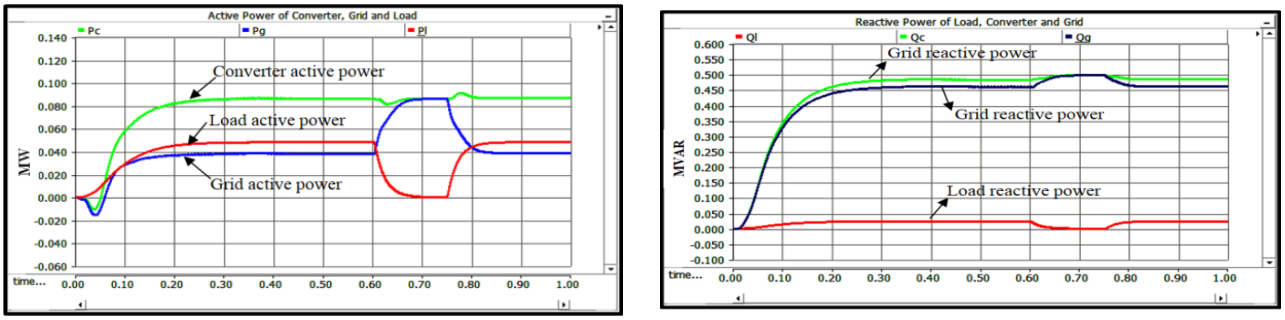

(a) (b)

Fig. 10 a) Active power of the converter, grid and load and b). Reactive power of the converter, grid and load.

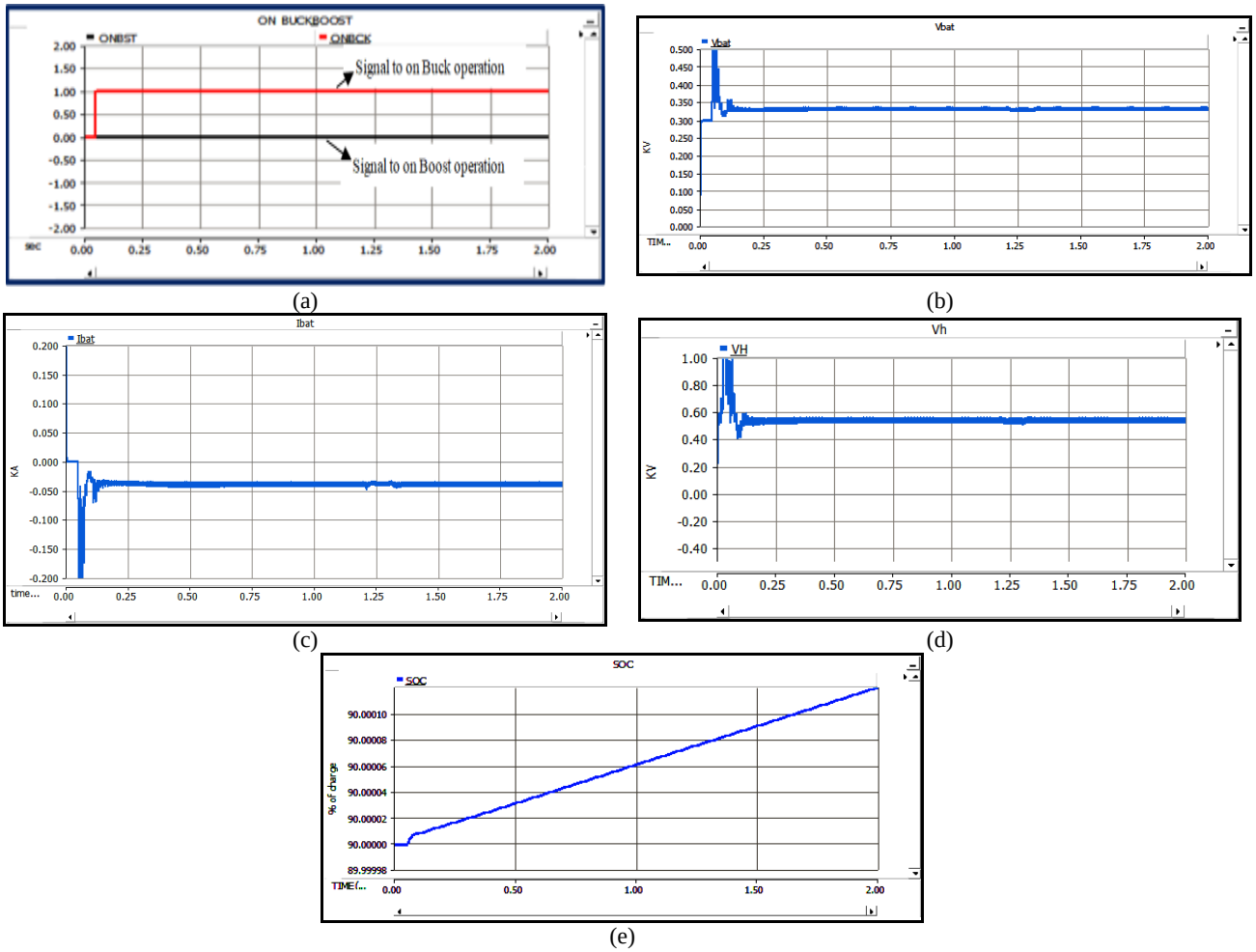

(a) (b) (c) (d) (e)

Fig. 11 a) Pulses to the lower controller from SOC (upper) controller, b) Voltage across the battery terminals, c) Current through the battery terminals, d) Voltage across the C_h of the charge controller, and e) State of charge (SOC) of the battery.

The charging and discharging states are observed with the help of the controller operation shown in Fig. 11(a). Figs. 11(b) and (c) indicates the voltage and current of the battery. Here the current in negative indicates the state of charging. The input voltage is maintained at 300V. From Fig. 11(d), the voltage across C_h the charge controller secondary side voltage and it is also the voltage across the dc link. The state of charge of battery is observed from Fig. 11(e) which indicates the charging mode rising from its 90% SOC (taken initial value) to above value. This part of simulation represents only the charging state of the battery. Hence it can be concluded that the active power and reactive power are balanced properly using the controller.

5.2 Case2: Load Disconnected With Battery Alone as a Source

During this operation, the battery acts as a source. The battery performs both charging and discharging operations, shown in Fig. 12(a).

The SOC curve from Fig. 12(b) which indicates charging and discharging of the battery system. In the absence of the PV system, the SOC indicates discharging. From Fig. 12(c), it is clear that the power flow is balanced between load, grid and converter. During the period of 0.6 to 0.8sec, the PV is in off state, during this battery supplies a part of the power to load and rest to the grid. After this instant, PV sets to operate and battery now starts charging. From Fig. 12(d) the reactive power flow between load, grid and converter are observed. The system is in stable operation for any sudden disconnection of load during a particular time period. During the period from t = 1.25s to 1.5s, the load is turned off and the converter power is supplied to the grid. It implies that the power balance between load, converter and grid is maintained as observed form Fig. 12(c) and Fig. 12(d). The system is said to be stable. Fig. 12(e) and (f) represents the individual THD's of voltage and current of each phase of the system. The THD of the voltage and current of the overall system are V_{THD}(0.0299) and I_{THD}(0.01) are maintained within the *IEEE* 519 standard.

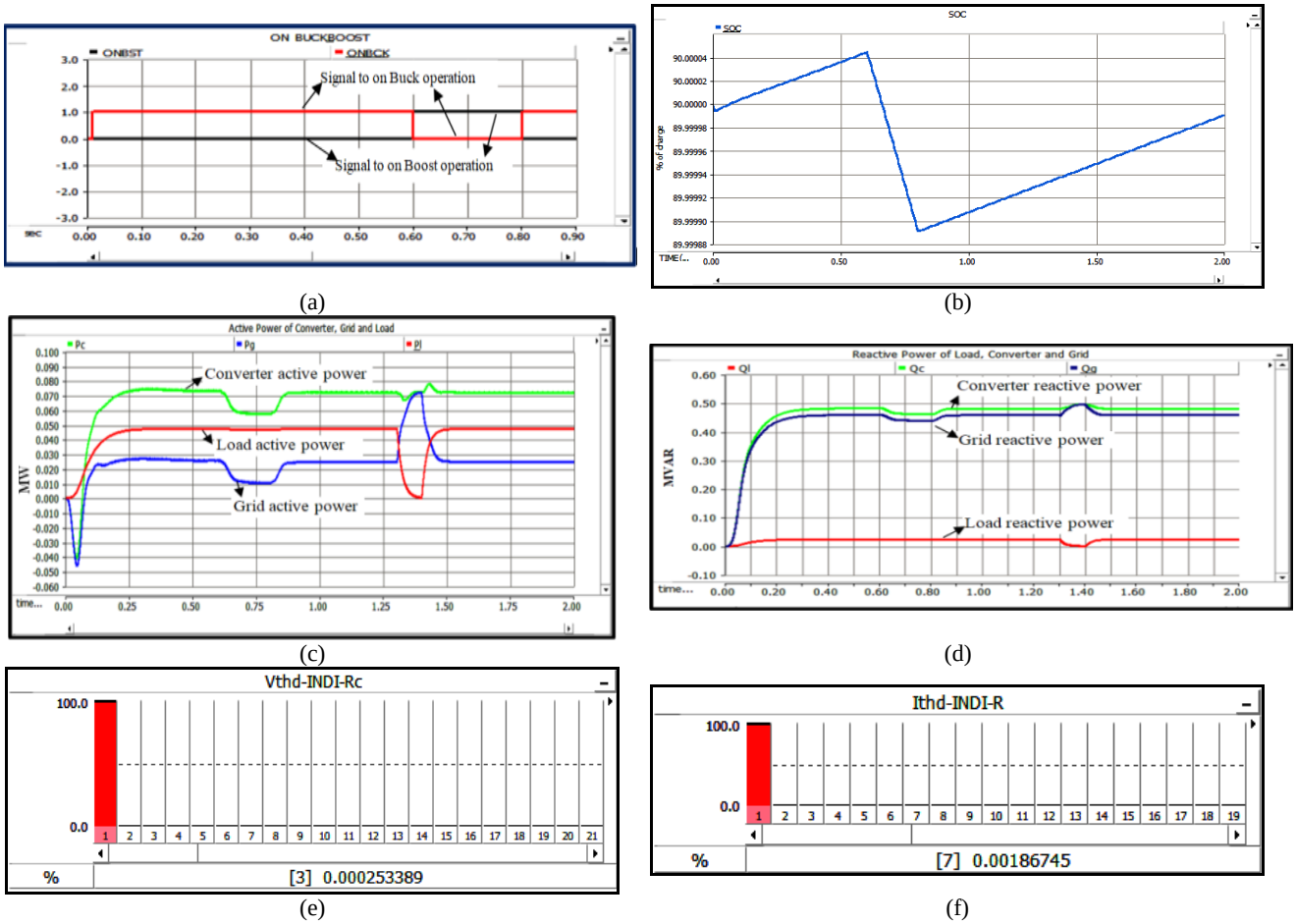

Fig. 12 a) On/Off pulses to the lower controller from SOC (upper) controller, b) State of charge (SOC) of the battery, c) Active power of the converter, grid and load, d) Reactive power of the converter, grid and load, e) Individual THD's of voltage, and f) current waveform of R-phase.

6 Single-Phase T-Type MLI System and Comparison with a Two-Level Inverter

6.1 Case 1: Battery as a Source of Power

Battery with boost converter used for obtaining high voltage level and constant lower voltage level is considered. The T-type multilevel inverter is operated with different modulation indexes of 0.7, 0.8, 0.9, and 1 for different power factors 0.7, 0.8, and 0.9. From Table 2 the current stress on the front end boost converter at different power factors with different modulation indexes are tabulated. These are compared with a two-level (2L) inverter. The T-type inverter has less current stress on switches and hence the requirement of cooling is very much reduced. Also higher output current ratings can be achieved. The switch in the converter is capable of increasing the power rating of the boost converter by increasing the current rate at the input side of the dc to dc converter. The rating of the current flowing through the switches in the T-type converter is nearly half the rating of the conventional converter at different power factors and is shown in Table 3.

The rate of change of current on front end boost converter switch is more in conventional two-level inverters compared to the T-type converters. The stress at different power factors with different modulation indexes are shown in Tables 4 and 5. The DC-DC converter used in the T-type converters has less rate of change of current stress, so the converter performance is better than the DC-DC converter used in the conventional inverter. The amount of stress in T-type is half compared to the conventional inverter which are tabulated in Table 4. The voltage stress on individual switches are half of the amount than the conventional H-bridge inverter. The inverter will be able to give a higher power rating than the conventional inverter by increasing the input DC voltage. The current stress on the individual switches are observed at different load power factors and also with different modulation index's. The average values of the currents are tabulated for both two-level and three inverters. It was shown as zero Amperes in Table 7. At 0.9 lagging power factor the load draws high current compared to 0.7 and 0.8 power factor, this is observed in both T-type and conventional converters. The amount of current stress is high in case of conventional inverters. If the load draws higher values of amperes, the switches will be affected and the amount heat dissipation increased. The T-type converters are capable to withstand for increment in the current drawn by the loads. The total harmonic distortion of the output voltage is tabulated and it is compared with the conventional inverter at different power factors. At each instant the T-type has very less (approximately 20%) THD than the conventional converter which is shown in Fig. 13. THD of the output current is tabulated and is compared with the conventional inverter at different power factors. At each instant the T-type has very less THD than the conventional converter by 20%.

Table 2 Current stress - front end boost converter.

I-Stress [Amps.] on Boost converter Switch at different power factors								
Modulation index	0.7		0.8		0.9		1	
	2L	3L	2L	3L	2L	3L	2L	3L
0.7 PF	14.26	5.2	14.19	7.32	13.12	8.96	13.1	10.98
0.8 PF	14.2	5.2	13.21	7.24	13.1	8.82	12.8	10.6
0.9 PF	13.5	5.1	13.1	7.15	13	8.77	12.7	10.5

Table 3 Rate of change of current [A/sec] - boost converter switch.

		$\frac{di_s}{dt}$ [A/sec]			
Power Factor	MI	0.7	0.8	0.9	1
0.7 PF	3L	3.21	6.81	10.92	16.96
	2L	12.66	17.16	22.01	24.77
0.8 PF	3L	4.8	8.97	13.17	21.71
	2L	14.02	18.61	24.25	29.02
0.9 PF	3L	4.39	9.5	16.44	24.93
	2L	19	23.93	29.56	31.93

Table 4 Voltage stress on individual Switches of inverter [V].

	VS1	VS2	VS3	VS4	VL1	VL2
2L	400	400	400	400	-	-
3L	200	200	200	200	200	200

Table 5 Current stress [A] at 0.9 PF.

Modulation index	0.7		0.8		0.9		1	
	2L	3L	2L	3L	2L	3L	2L	3L
Is1	18.1	14.5	16..04	13.3	15.8	12.7	15.4	12.7
Is2	18.1	16.3	16.04	14.3	15.8	14.2	15.4	14.06
Is3	18.1	14.5	16.04	13.3	15.8	12.7	15.4	12.7
Is4	18.1	16.3	16.04	14.3	15.8	14.2	15.4	14.06
I_L1	0	7.38	0	5.55	0	5.7	0	6.4
I_L2	0	7.38	0	5.55	0	5.7	0	6.4

Table 6 Current stress [A] at 0.8 PF.

Modulation index	0.7		0.8		0.9		1	
	2L	3L	2L	3L	2L	3L	2L	3L
Is1	18.12	14.2	16.03	13.3	15.26	12.5	15.5	12.5
Is2	18.12	15.9	16.03	14.5	15.26	13.9	15.5	13.7
Is3	18.12	14.2	16.03	13.3	15.26	12.5	15.5	12.5
Is4	18.12	15.9	16.03	14.5	15.26	13.9	15.5	13.7
I_L1	0	7.14	0	5.5	0	5.56	-	6.2
I_L2	0	7.14	0	5.5	0	5.56	-	6.2

Table 7 Current stress [A] at 0.7 PF.

Modulation index	0.7		0.8		0.9		1	
	2L	3L	2L	3L	2L	3L	2L	3L
Is1	18.08	14.6	15.98	13.48	15.39	12.5	15.4	12
Is2	18.08	16.3	15.98	14.57	15.39	14	15.4	14.2
Is3	18.08	14.6	15.98	13.48	15.39	12.5	15.4	12
Is4	18.08	16.3	15.98	14.57	15.39	14	15.4	14.2
I_L1	0	7.35	0	5.46	0	5.5	0	6.6
I_L2	0	7.35	0	5.46	0	5.5	0	6.6

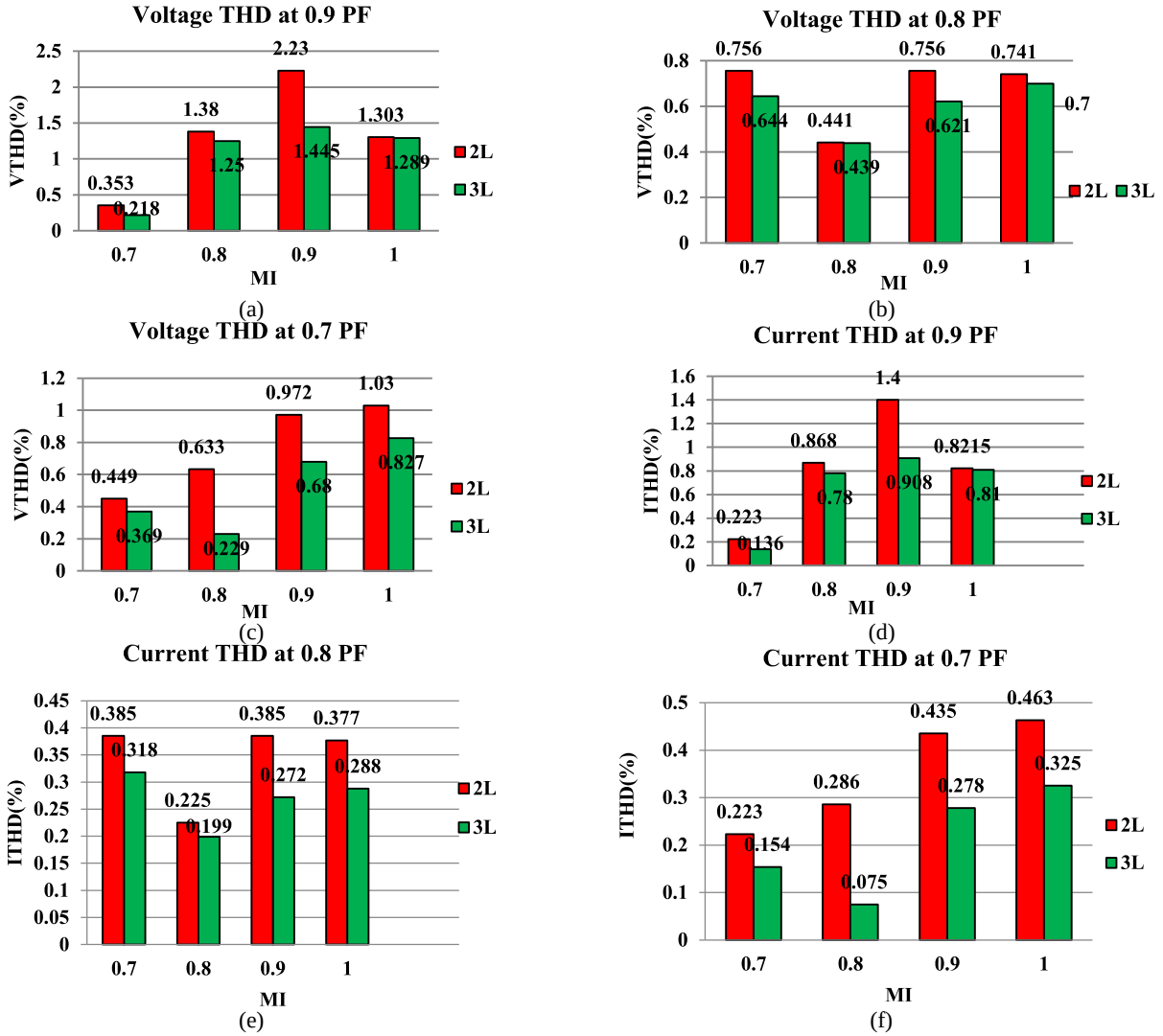

Fig. 13 Voltage THD at a) 0.9 power factor, b) 0.8 power factor, and c) 0.7 power factor; and current THD at d) 0.9 power factor, e) 0.8 power factor, and f) 0.7 power factor.

6.2 Case 2: Comparison of Conversion Efficiency for Single-Phase Two-Level and AS-MLI Inverters

The T-type has improvement in the overall efficiency by 2% of the system than the conventional converter which is shown in Fig. 14(a). At each modulation index (0.7, 0.8, and 0.9) the efficiency improvement is observed in T-type converters. The modulation index of 0.7 gives better improvement at each power factor condition. It is also observed that at 1.0 modulation index even the conventional inverters give better values, but the overall system enters into saturation region and also total harmonic distortion is increased. The THD is the main consideration in this work and so modulation index one is not preferred for comparison. At 0.7 power factor, the T-type converter efficiency is 3% more than the conventional inverter and 1% more at 0.8 power factor, and 2% more at 0.9 load power factor. In each case, the efficiency in the T-type converter gives better performance than the conventional H-bridge inverter. The filter values of the T-type inverter over the conventional inverter are tabulated in Table 8 for different power factors operating at different modulation indexes. The *LC* values are tuned properly to get the pure sine waveform and also to maintain rated RMS value at the output of the overall converter. There is a reduction in the values of the *L* and *C*. Hence cost and size of the filter are reduced. The conduction losses of the system are considered for analysis in order to focus on the heat dissipation of the overall system. The cooling requirement for the converter can be analyzed. The conduction losses of the converter switches at different switching frequencies are performed. The same analysis is done at different power factors. Figs. 14(b)-(d) represent the conduction losses.

From Fig. 14(b) it is clear that the losses are high by increasing the switching frequencies above 55 kHz (approx. 50W) in the two-level converters compared to the T-type converter at 0.9 power factor with 0.7 modulation index. At 0.8 modulation index it is 45W

Table 8 LC-filter values of the single-phase system at different power factors.

	MI	0.7		0.8		0.9		1	
Power factor		2L	3L	2L	3L	2L	3L	2L	3L
0.7 PF	*L* [mH]	12	8	12	8	13	12	14	12
	C [μF]	350	330	350	330	310	310	320	300
0.8PF	*L* [mH]	15	13	18	12	15	12	18	13
	C [μF]	320	320	330	310	320	300	320	300
0.9PF	*L* [mH]	18	14	14	12	13	12	14	13
	C [μF]	340	330	320	310	310	300	290	290

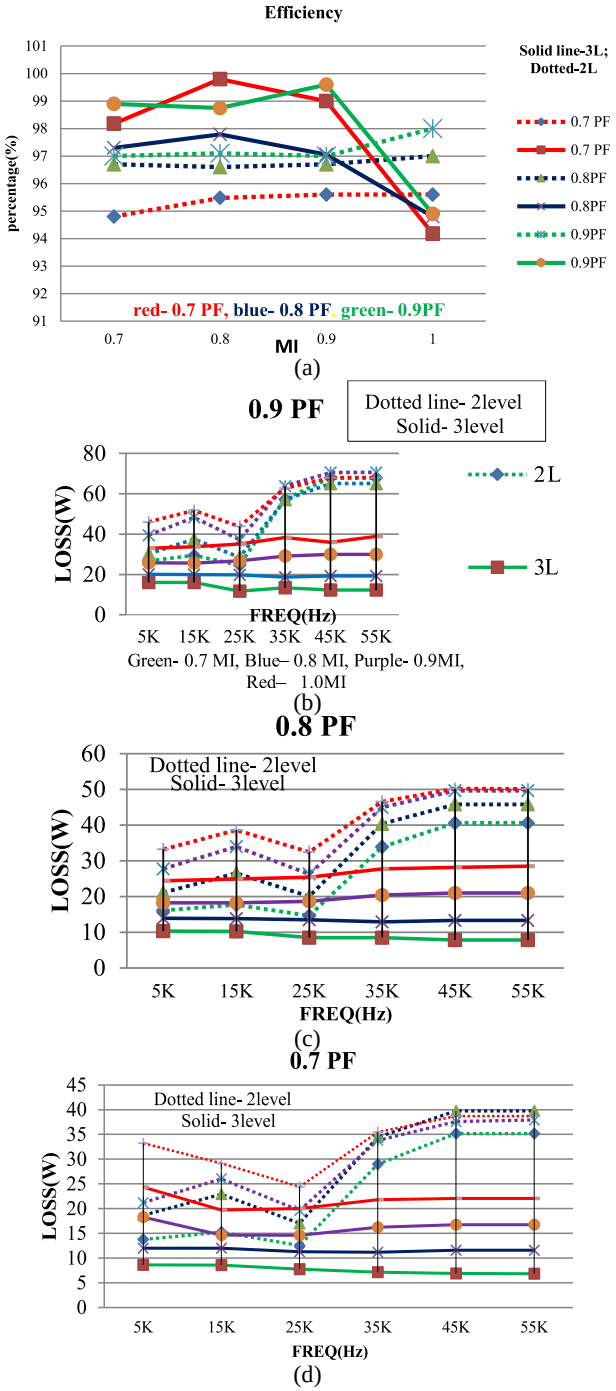

Fig. 14 a) System conversion efficiency at various power factors; Overall system switches conduction losses at b) 0.9 power factor, c) 0.8 power factor, and d) 0.7 power factor.

and at 0.9 modulation index it is 40W. At each power factor while going for higher switching frequencies, the converter losses of the overall system increase in a conventional two-level inverter. It is observed that total harmonic distortion for voltages and currents are within the limits of IEEE standard no 519 (1992) in both the cases discussed here. The T-type inverter shows better performance in all cases considered. It is preferable for the conversions from AC to DC or from DC to AC and can be used with renewable energy systems.

7 Conclusions and Future Scope

The design of the three-phase dual-port Asymmetrical T-type inverter and its interconnection to grid with two energy sources PV and Battery is explored. A vertical shift SPWM technique is used as a switching controller. Design of the front-end Boost converter, charge controller and filter parameters are presented. Its power regulation using *pq*-theory is performed. The power balance between inverter to load and the grid for load sharing is efficient. The battery is integrated with the designed inverter system and is charging (PV in operation) and discharging in absence of PV are performed. The charge controller is effective during absence of solar PV array. The power transfer to grid, when the load is shut down for a small period is studied. It is observed that the T-type inverter is a better replacement for the conventional H-bridge inverter for grid interconnection**.** It is also observed by the authors that the voltage and current stress on the front-end boost converter switch and also on the inverter is less. The conduction losses and THD are also less. The overall conversion efficiency is high. The size of the filter parameters required are reduced in T-type Asymmetrical MLI compared to a conventional inverter for grid interconnection.

A comparison with the conventional single-phase inverter is presented to validate the proposed inverter for grid interconnection with the help of case studies at different modulation indexes and at various power factors. The THD of voltage (2.9%) and current (1%) are very less in T-type inverter compared to the conventional inverter and are maintained within the permissible limits of IEEE -519 standards. This inverter is found to be more efficient and highly reliable compared to the conventional inverter circuit. This inverter finds application in back-back inter tie, induction heating, Reactive power compensation, adjustable speed drives, UPS, etc. The work can be extended with other renewable energy sources with different control algorithms. The DC-DC converters of the latest methodology (sepic/interleaved boost) also can be included. The battery charge controller can be understood with the latest algorithms.

References

[1] S. Kouro, J. I. Leon, D. Vinnikov, and L. G. Franquelo, "Grid-connected photovoltaic systems: An overview of recent research and emerging PV converter topology," *IEEE Industrial Electronics Magazine*, Vol. 1, No. 9, pp. 47–61, Mar. 2015.

[2] B. Sah and G. V. E. S. Kumar, "A Comparative study of different MPPT techniques using different DC-DC converters in a standalone PV system," in *IEEE Region 10 Conference (TENCON)*, Singapore, pp. 1690–1695, 2016.

[3] M. Killi and S. Samanta, "Modified perturb and observe MPPT algorithm for drift avoidance in photovoltaic systems," *IEEE Transactions on Industrial Electronics*, Vol. 62, No. 9, pp. 5549–5559, Sep. 2015.

[4] R. S. K. Athikamsetti and S. K. Gudey, "High power density parallel LC-link PV inverter for standalone and grid mode of operation," *Intelligent Computing Techniques for Smart Energy Systems*, Springer, Singapore, pp. 441–453, 2020.

[5] M. Shalini and S. K. Gudey, "Analysis and design of sliding mode control for MPPT based PV system with a battery storage," in *IEEE 14th IEEE India Council International Conference (INDICON)*, India, pp. 1–6, Dec. 2017.

[6] A. Sreedhar and S. K. Gudey, "Performance of a dual port Asymmetrical MLI with solar and battery using vertical shift SPWM," in *IEEE International Conference on Power Electronics, Drives and Energy Systems (PEDES)*, pp. 1–6, Dec. 2018.

[7] R. P. Eviningsih, M. Pujiantara, A. Priyadi, and M. Purnomo, "Controlled bidirectional converter using PID for charging battery in the stand-alone wind turbine system with modified P&O to obtain MPPT," *IEEE International Conference on Green Energy and Applications (ICGEA)*, pp. 69–75, Mar. 2017.

[8] X. Hu, C. Zou, C. Zhang, and Y. Li, "Technological developments in batteries," *IEEE Power & Energy Magazine*, 2017, pp. 20–31.

[9] M. Schweizer and J. W. Kolar, "Design and implementation of a highly efficient three-level T-type converter for low-voltage applications," *IEEE Transactions on Power Electronics*, Vol. 28, No. 2, pp. 899–907, Feb. 2013.

[10] F. Yang, H.Ge, J. Yang, R. Dang, and H. Wu, "A family of dual-buck inverters with an extended low-voltage DC-input port for efficiency improvement based on dual-input pulsating voltage-source cells", *IEEE Transaction on Power Electronics*, Vol. 33, No. 4, pp. 3115–3128, 2018.

[11] A. Zorig, M. Belkheiri, and S. Barkat, "Control of three-level T-type inverter based grid connected PV system," in *IEEE 13th International Multi-Conference on Systems, Signals & Devices (SSD)*, pp. 66–71, 2016.

[12] H. Wu, L. Zhu, F. Yang, T. Mu, and H. Ge, "Dual-DC-port asymmetrical multilevel inverters with reduced conversion stages and enhanced conversion efficiency," *IEEE Transactions on Industrial Electronics*, Vol. 64, No. 3, pp. 2081–2091, Mar. 2017.

[13] M. H. Rashid, *Power electronics circuits, devices and applications*. 3rd Ed. Englewood cliffs, NJ, USA: Prentice-Hall, 2004.

[14] G. J. Ruchiraj and P. N. Kapil, "Analysis of different modulation techniques for multilevel inverters," in *IEEE 1st International Conference on Power Electronics, Intelligent Control and Energy Systems (ICPEICES)*, pp. 1–6, 2016.

[15] G. L. Calzo, A. Lidozzi, L. Solero, and F. Crescimbini, "LC Filter design for on-grid and off-grid distributed generating units", *IEEE Transactions on Industry Applications*, Vol. 51, No.2, pp. 1639–1650, 2015.

[16] A. Reznik, M. G. Simoes, A. Al-Durra, S. M. Muyeen, "LCL filter design and performance analysis for grid-interconnected systems," *IEEE Transactions on Industrial Applications*, Vol. 50, No. 2, pp. 1225–1232, 2014.

[17] J. S. Lai and F. Z. Peng, "Multilevel converters- A new breed of power converters," *IEEE Transaction on Industry Applications*, Vol. 32, No. 3, pp. 509–517, Jun. 1996.

[18] M. H. Rashid, *Power electronics circuits, devices and applications*. 3rd Ed. Englewood cliffs, NJ, USA: Prentice-Hall, 2004.

[19] F. Z. Peng, "A generalized multilevel inverter topology with self-voltage balancing," *IEEE Transactions on Power Electronics*, Vol. 28, No. 2, pp. 730–739, Feb. 2013.

[20] S. Sabyasachi, V. B. Borghate, and S. K. Maddugari, "Step-wise design procedure for a single-phase multilevel inverter topology for different voltage level generation," *IET Power Electronics*, Vol. 12, pp. 729–738, Apr. 2019.

[21] M. H. Mondol, M. R. Tür, S. P. Biswas, M. K. Hosain, S. Shuvo, and E. Hossain, "Compact three-phase multilevel inverter for low and medium power photovoltaic systems," *IEEE Access*, Vol. 8, pp. 60824–60837, 2020.

[22] S. Pal, M. G. Majumder, R. Rakesh, K. Gopakumar, L. Umanand, D. Zielinski, and A. R. Beig, "A cascaded nine-level inverter topology with T-type and H-bridge with increased DC-bus utilization," *IEEE Transactions on Power Electronics*, Vol. 36, No. 1, pp. 285–294, Jan. 2021.

[23] V. K. Nagaboina and S. K. Gudey, "Design and analysis of a three phase transformer less hybrid series active power filter based on sliding mode control using PQ-theory and stationary reference frames", *Serbian Journal of Electrical Engineering*, Vol. 16, No. 3, pp. 289–310, Oct. 2019.

S. K. Gudey is working as a Professor in Gayatri Vidya Parishad College of Engineering (Autonomous), Visakhapatnam, Andhra Pradesh, India. He has graduated from JNTU Hyderabad in 2000, M.Tech from NIT Durgapur in 2002, and Ph.D. from NIT Allahabad in 2015. He has a teaching experience of 19 years. His research interests include modeling and control techniques for power electronics converters, power quality, renewable energy systems involving hybrid energy systems (solar, wind), microgrid operation and control. He is an SM of IEEE and a Life member of ISTE, India. He is having publications in reputed Journals like IET UK, Taylor and Francis, UK, and IEEE USA. He is a regular reviewer of journal articles in IEEE Transactions on Industrial Electronics, IEEE Transactions on Power Electronics, International Journal of Electronics, Taylor and Francis, Elsevier Science.

S. Andavarapu is a postgraduate student of Gayatri Vidya Parishad College of Engineering (Autonomous). He has completed his graduation in the year 2018. His areas of work include multilevel inverters and solar power grid integration. Presently he is planning for his Ph.D. work. He is good in PSCAD simulation and mathematical analysis of distribution system networks.